

# Emissions of methane from coal, thermal power plants and wetlands and its implications on atmospheric methane across the South Asian region

Mahalakshmi Venkata Dangeti<sup>1</sup>, Mahesh Pathakoti<sup>1\*</sup>, Kanchana Lakshmi Asuri<sup>1</sup>, Sujatha Peethani<sup>2</sup>, Ibrahim Shaik<sup>1</sup>, Rajan Sundara Krishnan<sup>3</sup>, Vijay Kumar Sagar<sup>4</sup>, Raja Pushapanathan<sup>5</sup>,  
5 Yogesh Kumar Tiwari<sup>4</sup>, Prakash Chauhan<sup>1</sup>

<sup>1</sup>National Remote Sensing Centre (NRSC), Indian Space Research Organisation (ISRO), Hyderabad, India-500037

<sup>2</sup>Formerly at The International Center for Agricultural Research in the Dry Areas

10 <sup>3</sup>Lab for Spatial Informatics, International Institute of Information Technology (IIIT), Hyderabad-5000084, India

<sup>4</sup>Indian Institute of Tropical Meteorology (IITM), Pune, India-411008.

<sup>5</sup>ICAR-Indian Institute of Soil and Water Conservation, Research Centre, Koraput, Odisha, India-763 002.

15

\*Corresponding author: mahi952@gmail.com

## Abstract

Atmospheric methane (CH<sub>4</sub>) is a potent climate change agent responsible for a fraction of global  
20 warming. The present study investigated the spatio-temporal variability of atmospheric column-  
averaged (*X*) CH<sub>4</sub> concentrations using Greenhouse gases Observing SATellite (GOSAT) and  
TROPOspheric Monitoring Instrument onboard the Sentinel -5 Precursor (S5P/TROPOMI) data  
from 2009 to 2022 over the South Asia region. During the study period, the long-term trends in  
*X*CH<sub>4</sub> increased from 1700 ppb to 1950 ppb with an annual growth rate of 8.76 ppb year<sup>-1</sup>.  
25 Among all natural and anthropogenic sources of CH<sub>4</sub>, the rate of increase in *X*CH<sub>4</sub> was higher  
over the coal site at about 10.15±0.55 ppb year<sup>-1</sup> (Paschim Bardhaman) followed by Mundra  
ultra mega power plant at about 9.72±0.41 ppb year<sup>-1</sup>. Most of the wetlands exhibit an annual  
trend of *X*CH<sub>4</sub> more than 9.50 ppb year<sup>-1</sup> with a minimum rate of 8.72±0.3 ppb year<sup>-1</sup> over Wular  
Lake. The WetCHARTs-based emissions of CH<sub>4</sub> from the wetlands were minimal during  
30 the winter and pre-monsoon seasons. Maximum CH<sub>4</sub> emissions were reported during the  
monsoon with a maximum value of 23.62±3.66 mg m<sup>-2</sup> month<sup>-1</sup> over the Sundarbans wetland.  
For the 15 Indian Agroclimatic zones, significant high emissions of CH<sub>4</sub> were observed over the  
Middle Gangetic Plains, Trans Gangetic Plains, Upper Gangetic Plains, East Coast Plains &  
Hills, Lower Gangetic Plains and East Gangetic Plains. Further, the bottom-up anthropogenic  
35 CH<sub>4</sub> emissions data are mapped against the *X*CH<sub>4</sub> concentrations, and a high correlation was  
found in the Indo Gangetic Plains region, indicating the hotspots of anthropogenic CH<sub>4</sub>.

40

**Keywords:** GOSAT, S5P/TROPOMI, Column-averaged CH<sub>4</sub>, South Asia, spatio-temporal,  
anthropogenic emissions.

## 1. Introduction

Atmospheric methane ( $\text{CH}_4$ ) is one of the high-potential greenhouse gases (GHG) and plays a vital role in the chemistry of the atmosphere. In the troposphere,  $\text{CH}_4$  oxidation is due to hydroxyl (OH) radical and produces carbon monoxide, carbon dioxide, and ozone in the presence of increased amounts of oxides of nitrogen. In contrast, in the stratosphere, oxidation of  $\text{CH}_4$  is by OH radical, atomic oxygen and chlorine (Nair and Kavitha, 2020).  $\text{CH}_4$  has enormous potential for global warming, about 28 times that of  $\text{CO}_2$  over 100 years (IPCC, 2021), and a comparatively short perturbation lifespan of about 12 years (Balcombe et al., 2018). Over the past decade, the research community has become more interested in anthropogenic  $\text{CH}_4$  concentration due to its persistent rise in the atmosphere, and lack of knowledge regarding its source or sink (Huang et al., 2015). The long-term  $\text{CH}_4$  observations from the National Oceanic and Atmospheric Administration (NOAA) have shown a yearly increase of 8 ppb year<sup>-1</sup>, while Shadnagar, an Indian site, shows an increase of 10 ppb year<sup>-1</sup> (Sreenivas et al., 2022). Though the emissions have increased over the past 20 years, the causes remain unclear. Recent research suggests that a combination of fossil fuel and agricultural emissions, with fluctuations in the  $\text{CH}_4$  sink in the atmosphere, also plays a part (Schaefer et al., 2016; Worden et al., 2017; Turner et al., 2019; Zhang et al., 2022). The decadal budget indicates that relative uncertainties may range from 20 to 35 % for inventories of anthropogenic emissions in specific sectors (agriculture, waste, fossil fuels), 50% for emissions from burning biomass and emissions from natural wetland ecosystems, and 100% or more for emissions from other natural sources which include inland waters and geological sources (Saunois et al., 2024). Maasackers et al. (2023) reported the annual gridded  $\text{CH}_4$  emission inventory over the United States of America (USA) while meeting the US Environmental Protection Agency (USEPA) emission inventory standards at 0.1°×0.1° spatial resolution. This data was submitted to the United Nations in 2020, reporting improved uncertainties over the global Emission Database for Global Atmospheric Research (EDGAR) database. Geographically, India's wetlands comprise 4.7% of the nation's total land area (Bassi et al., 2014; Kavitha et al., 2016). The primary sources of  $\text{CH}_4$  emissions include natural emissions from freshwater systems, wetlands, and geological sources; anthropogenic emissions come from waste management, agriculture, and the mining and burning of fossil fuels (Kirschke et al., 2013; Saunois et al., 2016a; Ganesan et al., 2019).

Wetlands are the natural sources that contribute 20 to 40% of global emissions and dominate the inter-annual variability (Parker et al., 2018). Only limited studies have been conducted in India about  $\text{CH}_4$  discharge from wetlands. A recent study (Vinna et al., 2021) shows that natural wetlands could produce 50% to 80% more  $\text{CH}_4$  emissions by 2100. According to Schlesinger et al. (2009), wetlands, rice paddies, and ruminants are the leading producers of  $\text{CH}_4$  on the Indian sub-continent. According to Hayashida et al. (2013), there is a seasonal pattern in the  $\text{CH}_4$  concentration over the Indian subcontinent, with higher values during the post-monsoon and minimum in pre-monsoon. Kavitha et al., (2016) used SCIAMACHY retrieved methane product over the Indian region to understand the spatio-temporal variations. The salient findings of this

study are that during monsoon and post-monsoon, high  $XCH_4$  values are observed in the Northern regions. Different seasonal behaviour is observed with seasonal peak in post-monsoon and low during monsoon in the Southern peninsular regions. These regional variations are due to the distribution of sources like livestock population, rice cultivation, wetland, biomass burning and oil and gas mining. Along with temperature, precipitation, and radiation, the  $CH_4$  emissions from the natural wetlands might affect the region's heat budgeting, exacerbating global warming on a local, regional, and even global scale (Sakalli et al., 2017). Thermal power plants are responsible for a large amount of the GHG emissions from the energy sector. Each thermal power plant has a different set of emission factors for methane and nitrous oxide, based on operating conditions and combustion technology (Kang et al., 2019). The integrated measure of  $CH_4$  includes contributions from the various vertical atmospheric layers, ranging from the Earth's surface measurement point to the uppermost layer of the atmosphere. Chandra et al. (2017) studied the raised air mass in the 600–200 hPa height layer over northern India, which accounts for 40% of the seasonal  $CH_4$  augmentation during the southwest monsoon season. Conversely, in the semi-arid region, the height over 600 hPa contributed up to approximately 88% of the amplitude of the  $XCH_4$  seasonal cycle, while the atmosphere below 600 hPa contributed only around 12%. The feature of air mass transport processes in the Asian monsoon region is the main reason for the increased contributions from above 600 hPa across the northern Indian region.

Insufficient datasets exist regarding the  $CH_4$  feedback originating from wetlands; a study on the precise estimation of  $CH_4$  outflow from wetlands and its impact on local/regional global warming scenarios is urgently needed. The ability to identify spatial and temporal fluctuations in atmospheric  $CH_4$  from space, due to recent technological developments in remote sensing, could help fill in the gaps left by measurements performed by ships, planes, and the ground (Frankenberg et al., 2008; Kuze et al., 2009; Kavitha et al., 2018). The present study focuses on the Implications of emissions from coal, thermal power plants, and wetlands on atmospheric methane over South Asia using  $XCH_4$  data from Greenhouse gases Observing SATellite (GOSAT) and TROPOspheric Monitoring Instrument onboard the Sentinel-5 Precursor (S5P/TROPOMI) from 2009 to 2022. It has further analyzed the spatial and temporal pattern of atmospheric  $CH_4$  variations and emissions and its correlation with anthropogenic  $CH_4$  emissions from the bottom-up emission inventory of the EDGAR. The wetland methane emissions were addressed using WetCHARTs v1.31. over the top 10 wetland sites of the present study. The response of atmospheric  $CH_4$  concentrations to anthropogenic emissions in various agroclimatic zones of India was further highlighted in this study using the  $XCH_4$  data from 2001 to 2022.

## 2. Study region

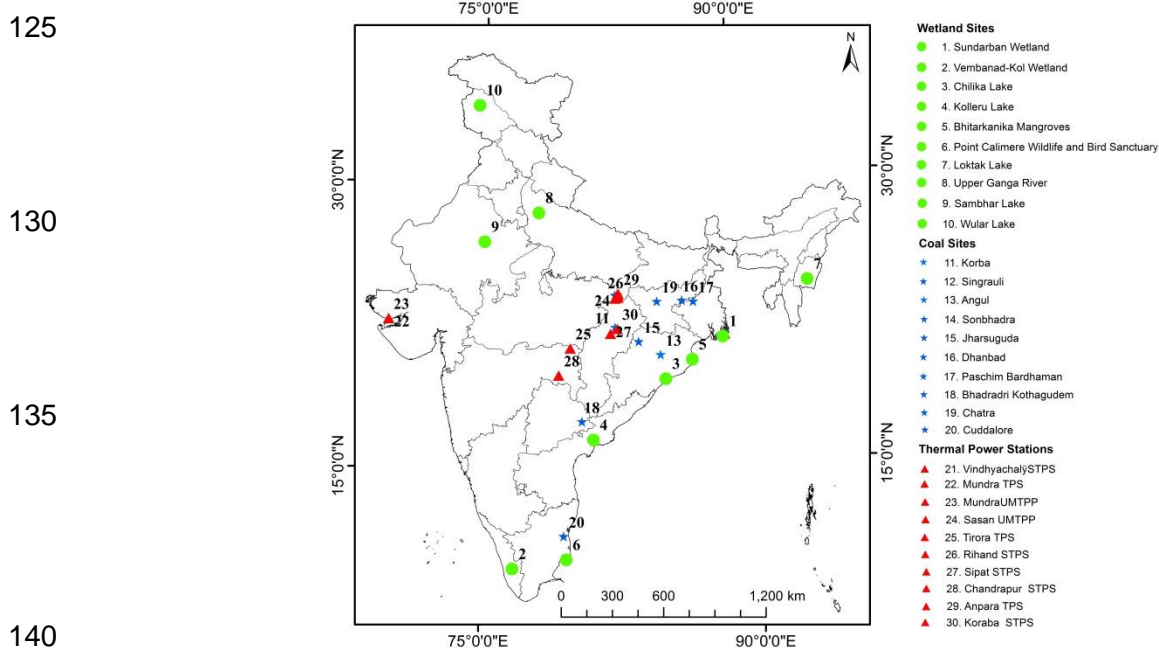


Figure 1. Study locations a) top 10 coal mine locations in India based on production capacity indicated by star (★); b) top 10 thermal power stations denoted by triangle (▲) and c) top 10 wetlands selected based on the area represented by circle (●).

The distribution of CH<sub>4</sub> sources over the Indian region is shown in Figure 1. The focus of the study was three CH<sub>4</sub> source regions—coal fields, thermal power plants, and the Ramsar wetlands. More details about Ramsar wetlands can be found below. . The number of coal mines in India varies from 1 to 65, and the top ten coal fields were selected for this study based on their production capacity. During 2019–2020, coal and lignite production was between 0.1 and 120.47 MT. The study's coal mine details are provided in Table 1. Similarly, Table 2 lists thermal power stations according to their respective power generation. The Ramsar Convention is an international agreement created in 1971 to protect wetlands and promote their sustainable use (<https://rsis Ramsar.org>). The Ministry of Environment, Forests and Climate Change (MoEF&CC), Government of India, has identified 75 Ramsar Wetland sites in India as of November 2022. These sites span a total area of 13,35,530 ha. Based on the high total geographical area coverage (Table 3), the top 10 places were determined for the current investigation. The size varies from 423000 ha (Sundarbans wetland, West Bengal) to 18900 ha (Wular Lake, Jammu and Kashmir) (<https://indianwetlands.in/wetlands-overview/indias-wetlands-of-international-importance/>; PIB Press Release on World Wetlands Day dated 26<sup>th</sup> August, 2022).

### 3. Data and Methodology

The GOSAT series developed by the Japan Aerospace Exploration Agency (JAXA) continuously monitors CO<sub>2</sub> and CH<sub>4</sub> from space (Kuze et al., 2009). The present study obtained the level 2 (L2) column CH<sub>4</sub> (XCH<sub>4</sub>) from the GOSAT. Onboard the GOSAT, the Thermal and Near Infrared (NIR) Sensor for Carbon Observation Fourier-Transform Spectrometer (TANSO-FTS) is used to detect the CO<sub>2</sub> and CH<sub>4</sub> absorption spectra in the shortwave IR (1.60μm & 2.0μm) region (Kuze et al., 2009; Kavitha et al., 2018). Ground-based FTIR measurements of XCH<sub>4</sub> by the Total Carbon Column Observing Network (TCCON) are used extensively to validate the GOSAT retrievals. Retrieval bias and precision of column abundance from GOSAT SWIR observations have been estimated as approximately 15-20 ppb and 1%, respectively (Morino et al., 2011; Yoshida et al., 2013). In the present study, the atmospheric CH<sub>4</sub> was obtained from 2009 to 2022 within a 100 km radius of the coal mines. The data corresponding to the quality flag (=0) was considered for the study only.

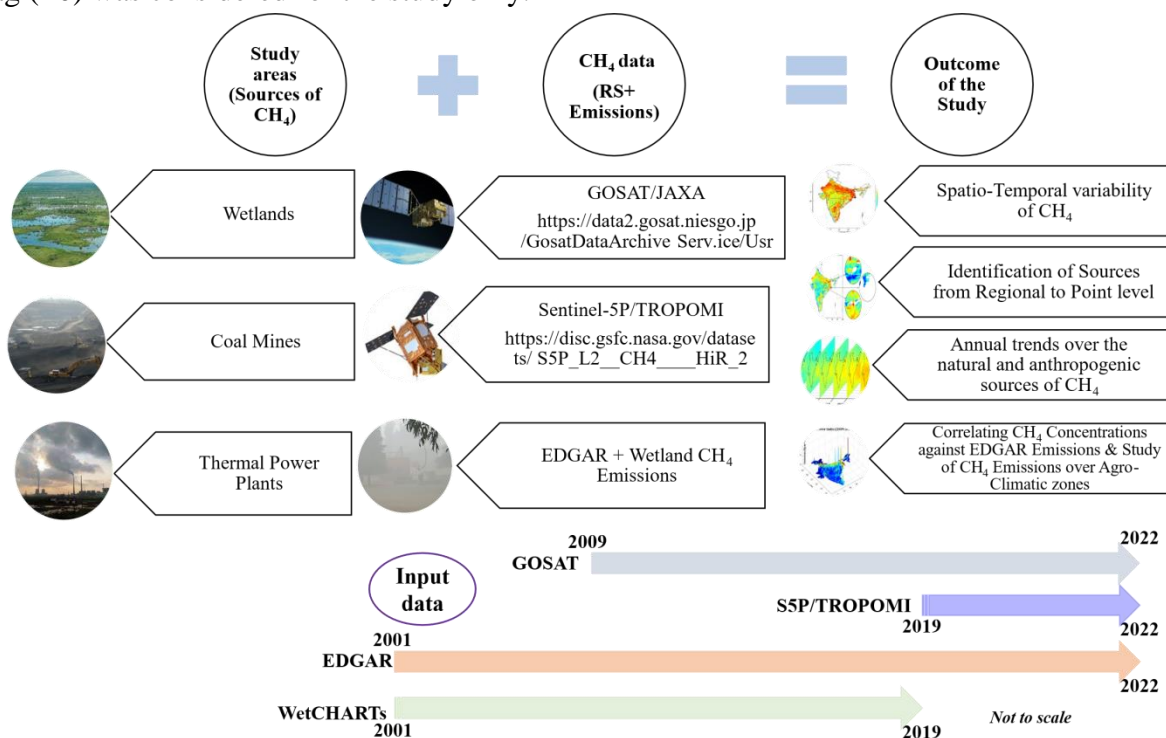


Figure 2. Data resources and study approach

The Sentinel-5 Precursor satellite, launched on October 13, 2017, is equipped with the TROPospheric Monitoring Instrument (TROPOMI), which tracks cloud characteristics, aerosols, and trace gases (Sentinel-5p. 2019). With a daily pass time of approximately 13:30 local solar time, the instrument's spectrometer measures reflected sunlight in the ultraviolet, visible, NIR, and SWIR spectral windows. The CH<sub>4</sub> retrieval algorithm uses the two spectral bands, i.e., reflectance in NIR (757-774 nm) and SWIR (2305-2385 nm) (Kozicka et al., 2023). Initially, retrievals based on TROPOMI had a spatial resolution of 7×7 km<sup>2</sup> (along-track x

across-track, Lorente et al., 2021). From August 2019 to the present, the resolution has been increased to  $5.5 \times 7 \text{ km}^2$  (Sagar et al., 2022). The latest data version is now v2 from 2021-07-01 to now. The quality flag ( $<0.5$ ) was only considered as per the product readme file document (Sentinel-5p. 2019). Methane retrieval from TROPOMI agrees with ground based FTIR  $XCH_4$  retrievals from TCCON and the Network for Detection of Atmospheric Composition Change (NDACC). The systematic differences of the bias-corrected  $XCH_4$  data with respect to TCCON and NDACC data are, on average,  $-0.26 \pm 0.56\%$  and  $0.57 \pm 0.83\%$ , respectively (Song et al., 2023). The data within the coal mines and wetlands area are taken from 01<sup>st</sup> May 2018 to 30<sup>th</sup> April, 2022. The individual shape files were given for each wetland field, and the satellite passes within the area were considered for the current study. As shown in Figure 2, a detailed procedure is explained in this section. The present study utilized the total anthropogenic emissions from the EDGAR (<https://edgar.jrc.ec.europa.eu/gallery?release=v50&substance=CH4&sector=TOTALS>, accessed on 01<sup>st</sup> November 2023) respectively. Uncertainties in the information on source intensity, activity and other statistical data are the key parameters for the uncertainties in the EDGAR emission inventory (Janardanan et al., 2017). Bottom-up inventory uncertainties range between 20 and 35% for agriculture, waste and fossil fuel sectors; 50% for biomass burning and natural wetland emissions and 100% or higher for natural sources such as geological seeps and inland waters for global methane emissions (Saunois et al., 2024). Further, the present study also utilized wetland methane emissions ( $\text{mg m}^{-2}\text{month}^{-1}$ ) from WetCHARTs v1.3.1 ([https://daac.ornl.gov/CMS/guides/MonthlyWetland\\_CH4\\_WetCHARTs.html](https://daac.ornl.gov/CMS/guides/MonthlyWetland_CH4_WetCHARTs.html)) which is available at spatial resolution of  $0.5^\circ \times 0.5^\circ$  with monthly temporal resolution and scale factor utilized here is  $124.5 \text{ TgCH}_4\text{yr}^{-1}$ . We have selected the coal fields based on the production as shown in Table 1. The data on all coal mines in India, their production, and their location are available at Pai et al. (2021) and Halder et al. (2024). Each district has open cast or underground types of mines found in India, and the number of coal mines varies from 1 to 65. The coal/lignite production was 0.1 to 120.47 MT during 2019-2020. The details of the coal mines in the present study are summarized in Table 1, and locations are mapped in Figure 1.

215

220

S.No	District names	No. of Mines	Production (MT)	Latitude	Longitude
1	Korba	15	120.47	22.47	82.56
2	Singrauli	7	82.19	24.15	82.6
3	Angul	13	80.61	20.97	85.11
4	Sonbhadra	5	47.36	24.15	82.74
5	Jharsuguda	9	36.71	21.69	83.89
6	Dhanbad	51	31.25	23.76	86.46
7	Paschim Bardhaman	65	31.23	23.68	87.11
8	Bhadradi Kothagudem	14	30.16	17.57	80.58
9	Chatra	4	29.65	23.76	85.01
10	Cuddalore	3	23.46	11.55	79.5

Table 1. The district names, the total number of coal mines, total production, and their centroid (latitudes and longitudes) locations of mines in the respective districts.

225 The list is prepared based on the descending order of total production in each district in India. There are 262 thermal power stations with a full capacity of 229.335 Gigawatt (GW) and a total unit of 2689 in India, based on diesel, gas turbine, and steam as on March 31, 2020. Table 2 shows the list of thermal power stations.

S.No	Power Stations names	Installed Capacity (MW)	No. of Units	Latitude (N)	Longitude (E)
1	Vindhyachal STPS	4760	13	24.1	82.68
2	Mundra TPS	4620	9	22.82	69.55
3	Mundra UMTTP	4000	5	22.82	69.53
4	Sasan UMTTP	3960	6	23.98	82.62
5	Tirora TPS	3300	5	21.41	79.97
6	Rihand STPS	3000	6	24.03	82.79
7	Sipat STPS	2980	5	22.14	82.29
8	Chandrapur STPS	2920	7	20	79.3
9	Anpara TPS	2630	7	24.21	82.8
10	Korba STPS	2600	7	22.39	82.68

230 Table 2. Top 10 thermal power plants based on their capacity.

There are 11 new Ramsar sites identified in 2022 (total 75 sites) by the Ministry of Environment Forests and Climate Change (MoEF&CC), India, covering a total area of 1,093,636 ha 2022. The

235 present study considered the top 10 sites based on the high area coverage (Table 3) for the current study. The area ranges from 18900 ha (Wular Lake) to 423000 ha (Sundarban Wetland).

<b>S.No</b>	<b>Wetlands Location</b>	<b>Latitude (N)</b>	<b>Longitude (E)</b>	<b>Area (ha)</b>
1	Sundarban Wetland	21.77	88.71	423000
2	Vembanad-Kol Wetland	9.83	76.75	151250
3	Chilika Lake	19.7	85.35	116500
4	Kolleru Lake	16.61	81.2	90100
5	Bhitarkanika Mangroves	20.65	86.9	65000
6	Point Calimere Wildlife and Bird Sanctuary	10.31	79.63	38500
7	Loktak Lake	24.43	93.81	26600
8	Upper Ganga River	28.55	78.2	26590
9	Sambhar Lake	27	75	24000
10	Wular Lake	34.26	74.55	18900

Table 3. Top 10 Wetland fields based on their area coverage.

240

245

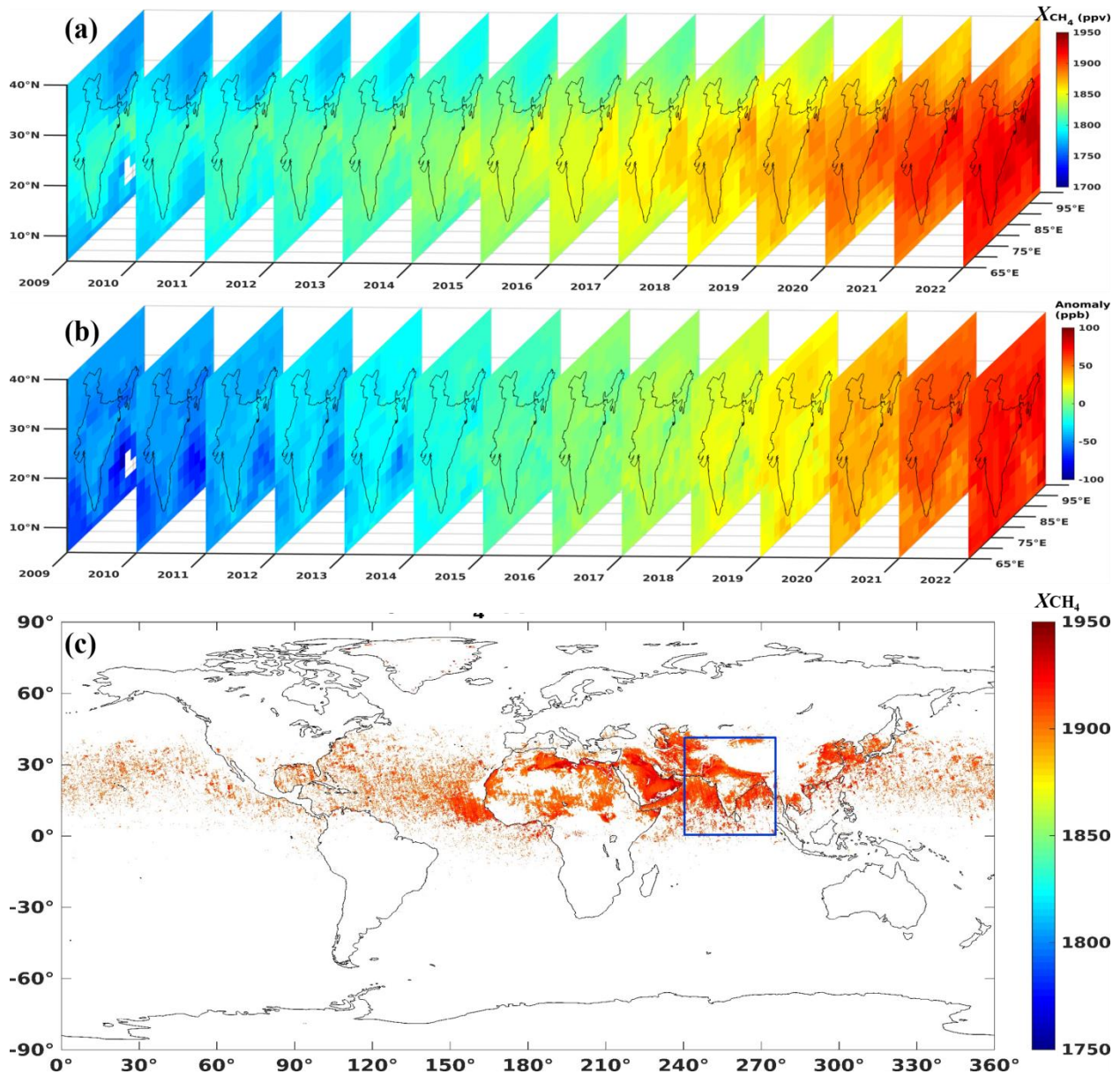
250

255



260 **4. Results and Discussion**

**4.1. Spatio-temporal variability of Space-based Atmospheric CH<sub>4</sub>**



265 Figure 3 a) Remote Sensing (GOSAT) of atmospheric CH<sub>4</sub> variability over the Indian sub-  
continent b) Anomaly during 2009 to 2022 and c) identification of probable high CH<sub>4</sub>  
concentration using S5P/TROPOMI data from 2019 to 2022 over the study region.

In the present study, we examined the annual space-time distribution of the XCH<sub>4</sub>, obtained from the GOSAT-1 and GOSAT-2 over South Asia as shown in Figures 3a-b from 2009 to 2022 (N=14 years)—the long-term trends in XCH<sub>4</sub> increased from 1700 ppb to 1950 ppb from 2009 to 2022 with an annual growth rate of 8.76 ppb year<sup>-1</sup>. This growth rate is statistically tested with a p-value less than 0.05 for n=3803 observations. A distinct, evident annual growth in CH<sub>4</sub> is seen

270

over the Indian subcontinent. Figure 3b shows the spatio-temporal residuals calculated using the data from 2009 to 2022. Residuals indicate that the acceleration of CH<sub>4</sub> emissions in India has been significant since 2015. Before 2015, the CH<sub>4</sub> concentrations were lower by 20 ppb to 50 ppb compared to the total mean of the study period, indicating a slow rise in CH<sub>4</sub> activities. However, post-2015, an increase of CH<sub>4</sub> was observed at a maximum of 100 ppb compared to the total mean, which indicates the surged emission rates from varied sources of CH<sub>4</sub> (Lu et al., 2023). To identify the critical potential high emission zones of CH<sub>4</sub>, the present study applied the 90<sup>th</sup> percentile statistical filter, as shown in Figure 3c. The percentile is often used to detect the points that are significantly different from the rest of the data. Statistically significant high concentrations of CH<sub>4</sub> are observed in tropical regions (Feng et al., 2023). In the blue highlighted box (Latitude: 0°-40° N and Longitude: 60°-100° E), higher concentrations of CH<sub>4</sub> were observed in the Indo-Gangetic Plain (IGP) and northwest (NW) areas of India, southeast of China, and NW of China. Southern China and north China are marked with wetlands and rice paddy fields, which are the primary sources of CH<sub>4</sub> (Kavitha et al., 2018; Chandra et al., 2019; Guo et al., 2023). High concentrations of CH<sub>4</sub> over the IGP and NW of India are due to the population density and various industries that contribute to the emissions of CH<sub>4</sub> and emissions from the rice paddy fields, respectively. In the present study, Figure 1 also shows the locations of coal and thermal power plants in India. Globally, the tropical wetlands ecosystem accounts for about 20% of the total global source (Saunois et al., 2020; Shaw et al., 2022), evidenced by bottom-up and top-down inventories. The study in the following sections assessed the CH<sub>4</sub> growth rate associated with the source type over the Indian region.

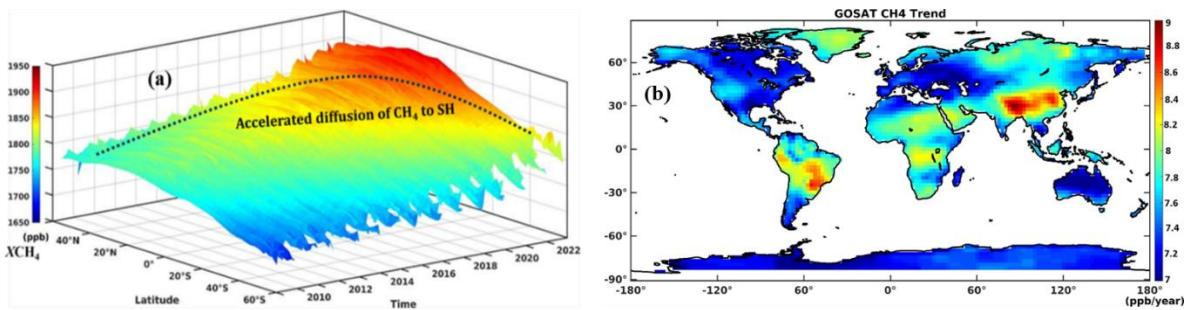


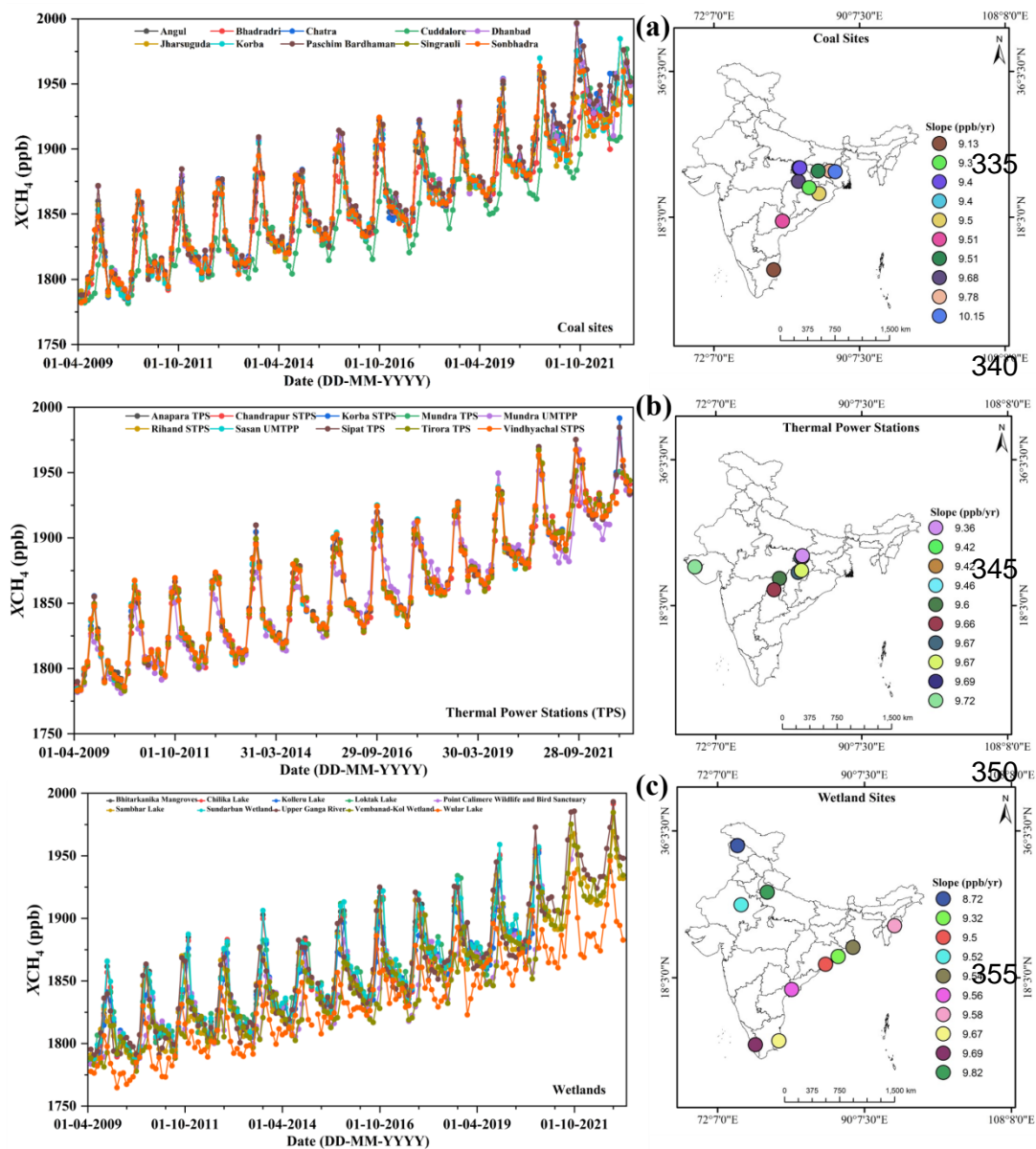
Figure 4. (a) Spatiotemporal distribution of annual XCH<sub>4</sub> as a function of latitude during 2010 to 2022. (b) Global XCH<sub>4</sub> trend (ppb year<sup>-1</sup>) using GOSAT data.

Figure 4 shows the spatiotemporal distribution of XCH<sub>4</sub> as a function of latitude, which depicts the annual variability at each latitude covering the northern and southern hemispheres (SH). There is a transparent latitudinal gradient in space. A strong diffusion of CH<sub>4</sub> is observed from the northern hemisphere to SH during 2009 to 2022. During 2010, the XCH<sub>4</sub> was distributed nearly constantly at all latitudes, indicating the stability of emissions from natural and anthropogenic sources. However, the gradient between the NH and SH has narrowed down with

a growth rate of 12 ppb year<sup>-1</sup> in 2022, reflecting the dominance of anthropogenic emissions over the tropics and unidentified leaks from the tropical wetlands and natural gas (Rocher-Ros et al., 2023). More thoroughly, the characteristics of regional and global spatiotemporal variations are revealed by the continuous XCH<sub>4</sub> data in space and time. As shown in Figure 4, it displays a latitudinal gradient, and each latitudinal zone's growth tendencies are comparable. Figure 4b shows XCH<sub>4</sub> has increased the global mean trend from 7 ppb year<sup>-1</sup> to 9 ppb year<sup>-1</sup>. There are hotspots in the XCH<sub>4</sub> trend observed in the Tibetan plateau (8.2 to 9 ppb year<sup>-1</sup>), South America (8.2 to 8.8 ppb year<sup>-1</sup>), and the African continent (8 to 8.4 ppb year<sup>-1</sup>), and in the rest of the world varies from 6.75 to 8 ppb year<sup>-1</sup>. Similarly high values were reported in the Tibetan plateau from 2010 to 2022 (Wei et al., 2019) and 8 ppb year<sup>-1</sup> (Song et al., 2023) from 2009 to 2021 using GOSAT data.

#### 4.2. Assessment of XCH<sub>4</sub> over different source types in India

Figures 5a-c show the monthly time series of XCH<sub>4</sub> over the specific sources of CH<sub>4</sub> plotted in the Indian region from 2009 to 2022. Over the Indian sub-continent and south-east Asia, October to November exhibits the highest amounts of CH<sub>4</sub>, while March through June often sees the lowest (Sreenivas et al., 2016; Song et al., 2023), because of the enormous diversity in the climate zones of the Asian region. The seasonal cycle (peak and trough) of XCH<sub>4</sub> is strongly associated with the vegetation during the active phase of cultivation and reduced photochemical reaction by the hydroxyl radicals, respectively. The major sink for CH<sub>4</sub> is by the oxidation of OH radical in the troposphere which removes 90% of CH<sub>4</sub> from the atmosphere (Crutzen et al., 1991). However, the potential available of OH radical in the atmosphere is not steady and changes rapidly depending upon the presence of solar ultraviolet radiation and other trace gases such as ozone, oxides of nitrogen (NO+NO<sub>2</sub>), and water vapor (Sreenivas et al., 2016).



360

Figure 5. Monthly time series of  $XCH_4$  over the a) wetlands, b) thermal power stations, and c) coal fields: sources of emissions, along with the overall growth rate at the respective site.

Over the coal, thermal, and wetlands, the  $XCH_4$  shows typical seasonal behavior, with maximum activity during the post-monsoon (October-November) and minimum activity in the pre-monsoon (March-May), as shown in Figure 6. A seasonal maximum of  $XCH_4$  was observed over

365

coal and thermal power plants from September to October and a minimum in pre-monsoon (March to May). In the case of wetlands, a shift in seasonal maxima varies from site to site, indicating their respective active phase of methanogens and the magnitude of the seasonal amplitude, which runs as a function of the individual wetland area. Methanogens are microscopic

370

organisms that break down organic substances in an oxygen-free environment. Thus, wetlands are perfect for methanogens to grow and release  $CH_4$  since they are usually oxygen-poor, moist

habitats (Zhang et al., 2023). Therefore, the present study investigated the above-listed wetlands. Most of the wetlands exhibit an annual growth rate of  $XCH_4$  greater than  $9.50 \text{ ppb year}^{-1}$  with high concentrations over Sundarbans wetland (Area = 423000 ha) with pronounced seasonality at all sites and lower concentrations over Wular Lake (area = 18900 ha) with an annual trend of  $8.72 \pm 0.3 \text{ ppb year}^{-1}$ .

During the examination period, the seasonal trends (slope) at each location, as summarised in Tables 1-3, were evaluated using Sen's slope-based Mann-Kendall test with a significance of  $p$ -value  $< 0.05$  (Pathakoti et al., 2021). The rate of increase in  $XCH_4$  was higher over the Upper Ganga (area = 26590 ha) with a slope of  $9.82 \pm 0.52 \text{ ppb year}^{-1}$  and followed by Vembanad-Kol Wetland (area = 151250 ha) with a slope of  $9.69 \pm 0.44 \text{ ppb year}^{-1}$ . Over the Sundarbans wetlands, West Bengal (area= 423000 ha) the rate of increase in  $XCH_4$  is  $9.54 \pm 0.51 \text{ ppb year}^{-1}$ . To investigate further, the present study quantified the source-based natural  $CH_4$  fluxes from each wetland using the WetCHARTs data in the following section.

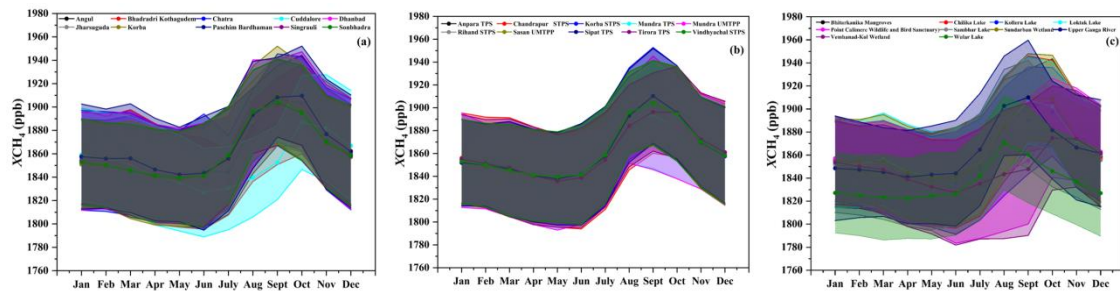


Figure 6. Seasonal  $XCH_4$  over a) coal fields, b) thermal power stations and c) wetlands.

Typically, the Indian climate is hot and humid, causing disturbances in the rainfall patterns; an increase in the waterlogged soils expands the wetlands (Zhang et al., 2023). Typical tropical wetlands are acting as positive feedback to climate change (Salimi et al., 2021). Irrespective of the power production capacity, over the thermal power plants, the  $CH_4$  exhibited stabilized seasonality at each location. However, the growth rate of  $XCH_4$  was higher over the Mundra Ultra Mega power plant (UMPP), Gujarat with a slope of  $9.72 \pm 0.41 \text{ ppb year}^{-1}$  followed by Mundra Thermal power station with a slope of  $9.69 \pm 0.4 \text{ ppb year}^{-1}$ . The Mundra TPS and UMPP, Gujarat have a total power capacity of 8620MW with 14 units. With 2630 MW installed power capacity the Anpara TPS exhibited an  $XCH_4$  growth rate of  $9.36 \pm 0.5 \text{ ppb year}^{-1}$ . This indicated the higher potential power plants contribute more  $CH_4$  emissions into the atmosphere. Over the coal mines, Paschim Bardhaman (31.23 MT, 65mines) shows a high  $XCH_4$  trend of about  $10.15 \pm 0.55 \text{ ppb year}^{-1}$  followed by Dhanbad (31.25 MT, 51mines), Korba (120.47 MT, 15mines) which shows  $XCH_4$  trend of  $9.78 \pm 0.53 \text{ ppb year}^{-1}$  and  $9.68 \pm 0.52 \text{ ppb year}^{-1}$ , respectively. Angul (80.61MT, 13 mines) and Chatra (29.65 MT, 4 mines) show  $XCH_4$  trend of  $9.51 \pm 0.5 \text{ ppb year}^{-1}$ . The lowest annual trend in  $XCH_4$  was observed over the Cuddalore coal mine (23.46 MT, 3 mines) which is about  $9.13 \pm 0.4 \text{ ppb year}^{-1}$ . Anthropogenic emissions

influence the methane growth trend. Wetland and biomass burning emissions determine the interannual variability (Fo et al., 2024). Figure 7 shows the continuous  $XCH_4$  data from the S5P/TROPOMI at  $0.05^\circ \times 0.05^\circ$ , complementing the GOSAT efforts in monitoring the  $XCH_4$  dynamics in space and time. We demonstrated the spatiotemporal variation characteristics of  $XCH_4$  more comprehensively at three different source type locations (wetland, coal, and thermal power plant). High  $XCH_4$  concentrations over the coal and thermal power station sites, and relatively lower concentrations in the wetland site. We concluded that the high-resolution S5P/TROPOMI has the potential to detect the point source variability. The growth rates of  $XCH_4$  over the wetlands compete with coal sites, indicating an equivalent anthropogenic source. Results of the analysis in the context of thermal power plants and coal mines indicate that the emissions from the fossil fuel industries are significant, and the release of  $CH_4$  into the atmosphere is commensurate with the production of the power and mining capacity.

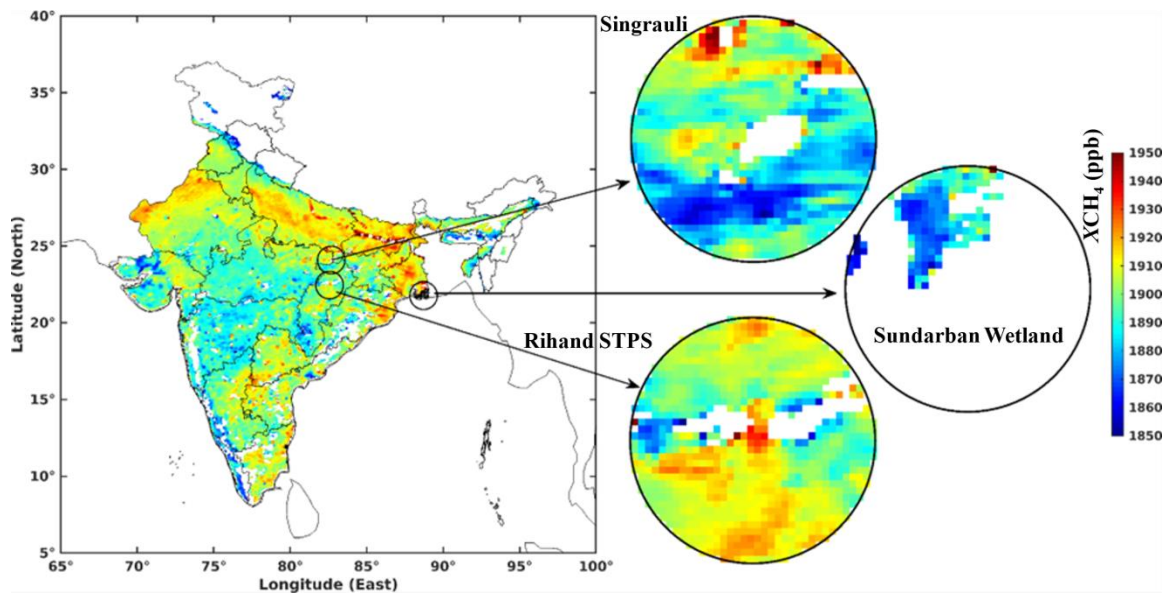


Figure 7. S5P/TROPOMI  $XCH_4$  gridded to  $0.05^\circ \times 0.05^\circ$  over Indian region and  $XCH_4$  over wetland, coal, and thermal power plant sites with a radius of 100 km.

### 4.3 $CH_4$ emission from India's wetlands

In addition to the anthropogenic emissions, the present study utilised the global monthly wetlands emission estimates from the Wetland Methane Emissions and Uncertainty (WetCHARTs v1.3.1) inventory (Bloom et al., 2017a, b; Bloom et al., 2021). The figure 8a shows the monthly  $CH_4$  emission over India's top 10 wetland sites from 2001 to 2019 and figure 8b represents the long-term seasonally averaged  $CH_4$  emission over wetlands. Emissions of  $CH_4$  from the wetlands were minimal in the winter season (December to February) and pre-monsoon (March to May). In the tropical region, winter and pre-monsoon seasons are considered dry months with moderate to high temperatures and less precipitation. A study by Peng et al. (2022) and Feng et al. (2022) hypothesized that warmer and wetter wetlands contribute significantly to the high  $CH_4$  emissions to the atmosphere. Typical climatological (1991-2020) mean temperature

(accumulated seasonal precipitation) over India during winter, pre-monsoon, monsoon, and post-monsoon are 20 °C (23 mm), 28 °C (98 mm), 26 °C (867 mm) and 23°C (106 mm) respectively  
 435 (https://climateknowledgeportal.worldbank.org/country/india/climate-data-historical). At all the wetland study sites during the study period, the maximum CH<sub>4</sub> emission was reported during the monsoon months with a maximum value of 23.62±3.66 mg m<sup>-2</sup> month<sup>-1</sup> over the Sundarbans wetland, which is the largest protected wetland of India and mangrove forest in the world. Besides climatic conditions, the emissions of CH<sub>4</sub> are positively correlated with the size of the  
 440 wetland, thus reporting maximum CH<sub>4</sub> emission over the Sundarbans site. High natural CH<sub>4</sub> emissions during the monsoon positively correlate with the atmospheric XCH<sub>4</sub> concentrations. Further, Mann-Kendall-based statistical analysis was carried out to assess the annual trend in the CH<sub>4</sub> emissions and found significant trend over the Wular Lake, with an increasing rate of 0.04 mg m<sup>-2</sup> year<sup>-1</sup> with a *p-value* of 0.01. An annual trend of XCH<sub>4</sub> was over this study is about  
 445 8.72±0.3 ppb year<sup>-1</sup>. The current research highlights the need for further investigation to correlate in detail the temperature and associated precipitation influence on methane oxidation and microbial activities, thus modulating the CH<sub>4</sub> emissions from the wetlands.

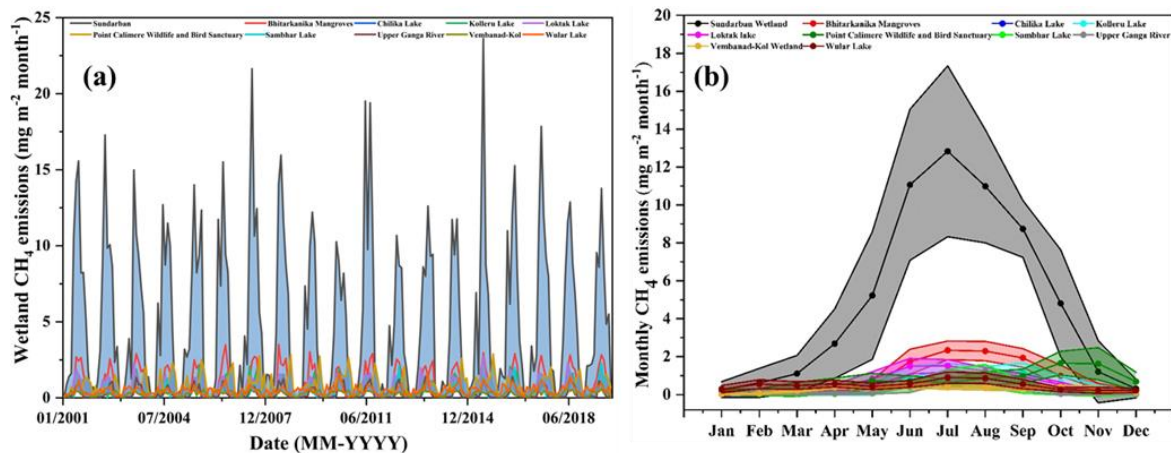


Figure 8. (a) Monthly Time series of Methane emissions (mg m<sup>-2</sup> month<sup>-1</sup>) over the wetland sites,  
 450 (b) Seasonal methane emissions over the wetland sites from 2001 to 2019.

455

460

#### 4.4 Long term seasonal winds over the source locations

465

470

475

480

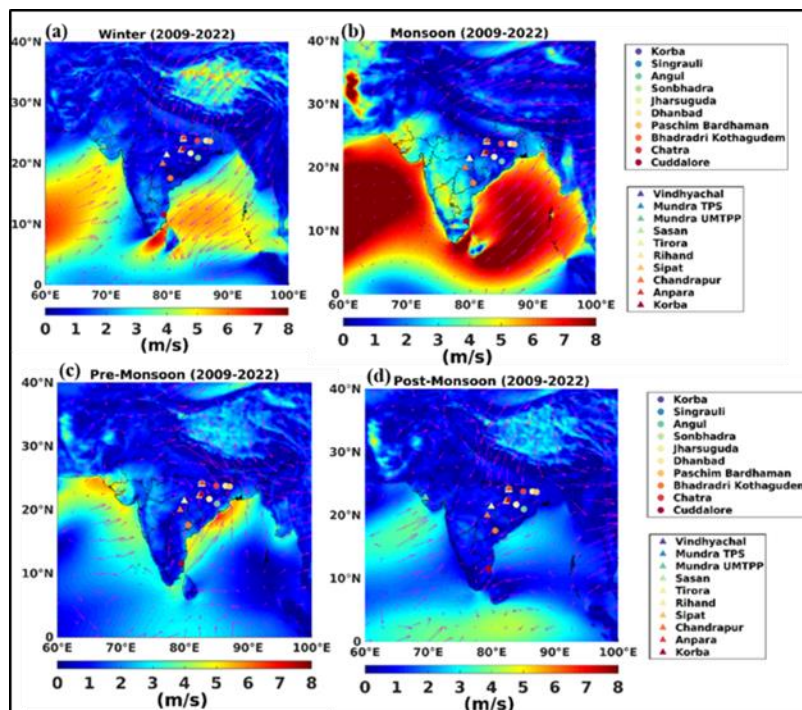


Figure 9. Long term seasonal winds for source types (coal and thermal power plants) for the period 2009-2022 (a) winter (b) Monsoon (c)Pre-monsoon (d) post-monsoon respectively.

485

490

495

The 10 m u wind component of wind from ERA5 which is reanalysis product is used in the present study for the period 2009-2022. The figure 9 shows the long-term seasonal winds for coal and thermal power plants for the period 2009-2022. During winter, winds are primarily from northeast (NE) direction with low wind speeds at the study locations. During monsoon and pre-monsoon majority of winds are from southwest (SW) direction with medium to high wind speeds arriving at the source locations. At the coal and thermal power plants, winds from the SW during the pre-monsoon, which transports relatively clean airmass from the ocean to land, could also influence the observed low CH<sub>4</sub> concentrations along with the continued source activity and seasonality. Quantification of CH<sub>4</sub> fluxes with an improved accuracy also needs required information about the prevailing winds at the source locations. Bussmann et al. (2024) established a detailed relationship between modulation in CH<sub>4</sub> fluxes against the wind speed and direction in his studies.

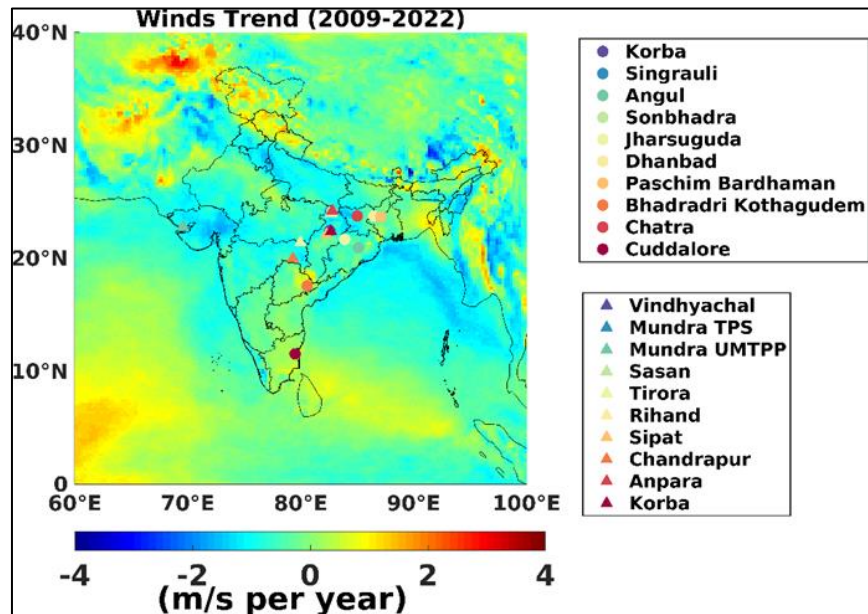
500



505

510

515



520 Figure 10. Long-term spatial trend of winds over the Indian region covering source types (coal and thermal power plants) for the period 2009-2022.

Figure 10 shows the trend in wind speeds over the coal and thermal power plants from 2009-2022. Around the coal mine sites, a positive trend in wind speed is observed over the Cuddalore coal mine site ( $0.42 \text{ ms}^{-1} \text{ year}^{-1}$ ), whereas the remaining coal mine sites show a negative trend in wind speed. The maximum negative trend is observed over the Sonbhadra coal mine site ( $1.21 \text{ ms}^{-1} \text{ year}^{-1}$ ), and the minimum negative trend is observed over the Bhadradi Kothagudem coal mine ( $0.18 \text{ ms}^{-1} \text{ year}^{-1}$ ). A negative trend in wind speed is observed over all the thermal power plants, with a maximum trend observed over the Vindhyachal STPS ( $1.23 \text{ ms}^{-1} \text{ year}^{-1}$ ) and a minimum over the Sipat STPS ( $0.63 \text{ ms}^{-1} \text{ year}^{-1}$ ). Over the wetland sites, a positive trend in wind speed is observed over the Point Calimere Wildlife and Bird Sanctuary ( $0.25 \text{ ms}^{-1} \text{ year}^{-1}$ ) and Wular Lake ( $0.20 \text{ ms}^{-1} \text{ year}^{-1}$ ). All the remaining wetland sites show a negative trend in wind speed. Besides the surface emissions, column  $\text{CH}_4$  values are also varied by the background flow advection and unstable boundary layer due to strong convection (vertical mixing) in the daytime (Ricaud et al., 2014; Francis et al., 2023). A negative trend is observed over the source locations in the present study, indicating relatively slower dispersion at these locations, thus modulating column  $\text{CH}_4$  values.

535

#### 4.5 $\text{CH}_4$ emissions over India's Agroclimatic zones

540 India is divided into 15 agroclimatic zones according to the combination of soil types and climatic conditions (Choudhary and Sirohi, 2022). These zones offer a structure for the nation's development and execution of agricultural policies and practices. The crops and farming

545 methods that are most appropriate for the environmental conditions in each zone are distinct from one another. Out of natural and anthropogenic sources of CH<sub>4</sub>, agricultural activity is also one of the dominant contributors to CH<sub>4</sub> dynamics in the atmosphere. Figures 11a-c show India's 15 agroclimatic zones and spatiotemporal trends of CH<sub>4</sub> emissions obtained from the bottom-up emission inventory of EDGAR (Crippa et al., 2020) from 2001 to 2022. Significant high emissions of CH<sub>4</sub>, as shown in Figure 11c, were reported over the Middle Gangetic Plains-MGP (2), Trans Gangetic Plains-TGP (3), Upper Gangetic Plains-UGP (4), East Coast Plains & Hills-ECPH (7), Lower Gangetic Plains-LGP (14) and East Gangetic Plains-EGP (15). These agroclimatic zones have active farming in rice, wheat, sugarcane, maize, millet, gram, cotton, etc. Besides traditional farming, the Lower Gangetic Plains has also actively contributed to livestock, horticulture, and forage production (Ahmad et al., 2017). Among all 15 agroclimatic zones, the MGP, TGP, UGP, ECPH, LGP and EGP have exhibited high emissions of CH<sub>4</sub> indicating the diversification of agricultural practices and homogenous traditions of agricultural production. Rice- wheat (R-W) based production system is mainly being practiced in this region which is causing negative effects on climate (Taneja et al., 2019). CH<sub>4</sub> emissions over the Northwest region are exhibiting weak contribution compared to other agroclimatic zones of India.

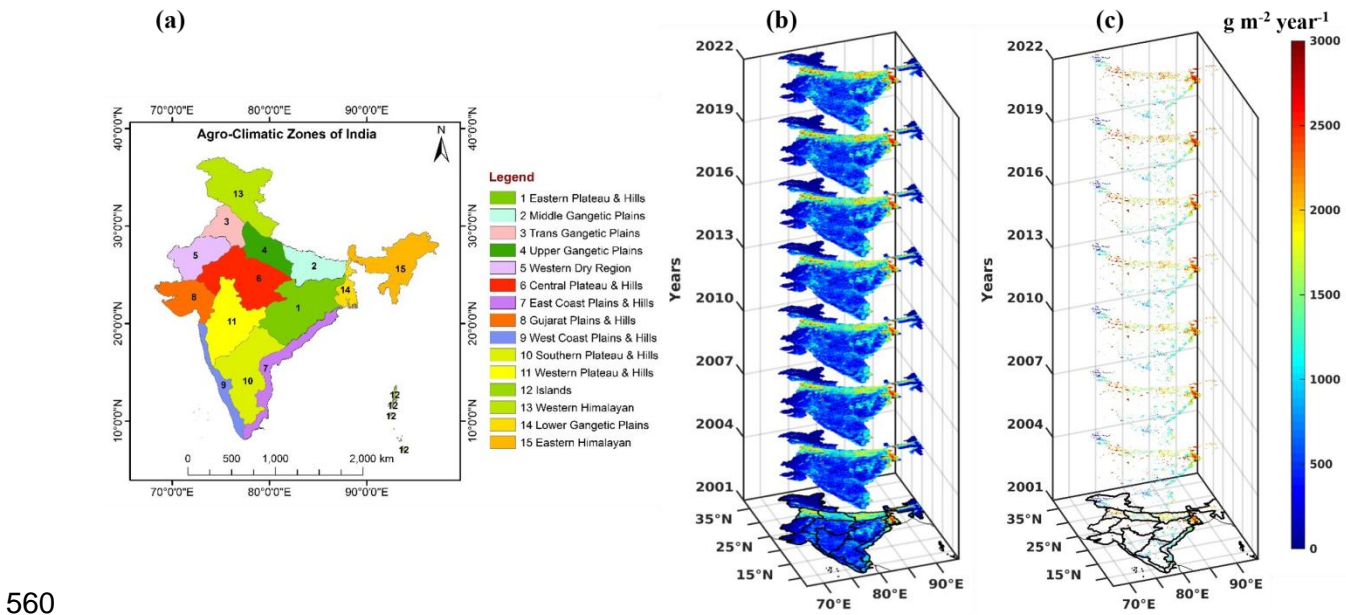


Figure 11. a) Agroclimatic zones of India, b) bottom-up CH<sub>4</sub> emissions inventory of EDGAR and c) 90<sup>th</sup> percentile statistical filter applied on CH<sub>4</sub> emissions from 2001 to 2022.

#### 565 4.6 Spatial correlation between XCH<sub>4</sub> concentrations and emissions over India

To understand the relationship between India's high XCH<sub>4</sub> concentration zones against emissions, we have computed pixel-level correlation between S5P/TROPOMI measured XCH<sub>4</sub> concentrations and bottom-up inventory of EDGAR-based XCH<sub>4</sub> anthropogenic emissions. Figures 12a-c shows XCH<sub>4</sub> concentrations from S5P/TROPOMI, EDGAR-based anthropogenic

570 emissions, and their correlation coefficient. The spatial patterns of  $XCH_4$  concentrations agree well with the high-emission regions. The correlation coefficient 'r' is strongly positive on in the IGP region, shows that more  $CH_4$  emission into the atmosphere through rapid industrial activity and anthropogenic contribution from human activity due to high population density. Besides the IGP region, the 'r' value is also strong in the east and northeast region due to the emissions from  
 575 natural sources such as agricultural activities, livestock, and wetlands (Behera et al., 2022).

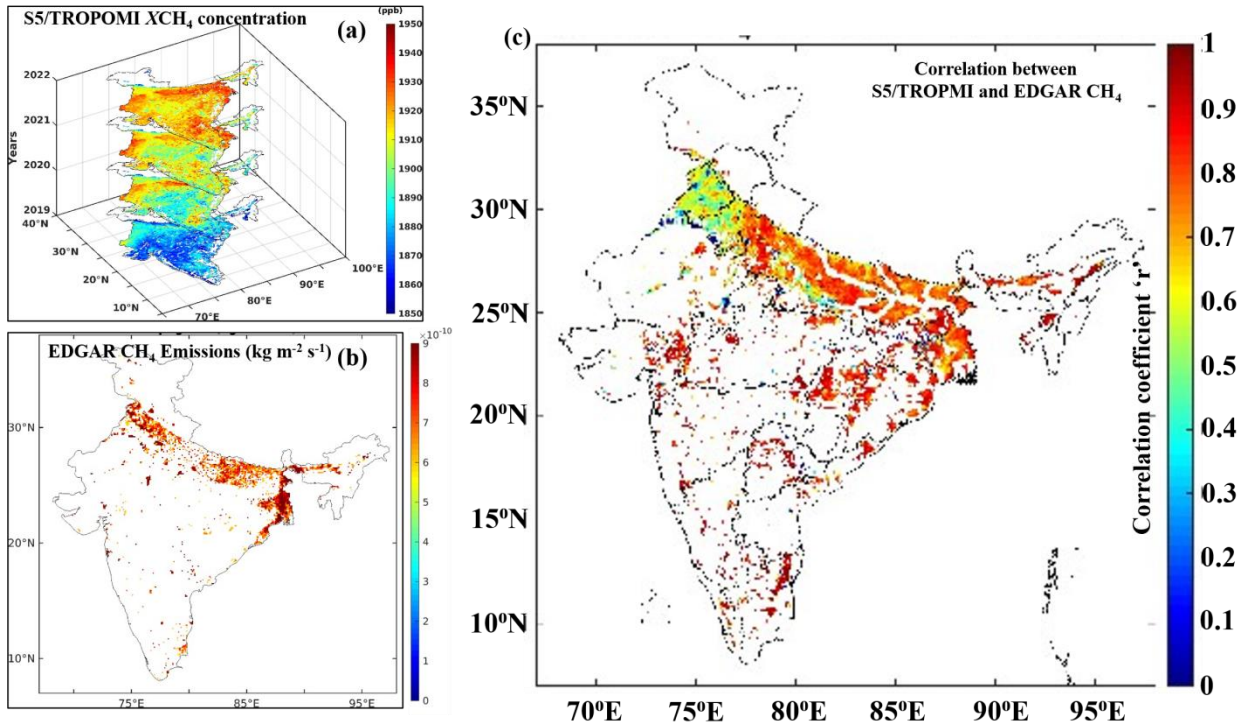


Figure 12. Pixel level correlation between S5P/TROPOMI based a)  $XCH_4$  concentrations and b) anthropogenic  $CH_4$  bottom-up emission inventory of EDGAR during 2019 to 2022 and c) correlation map.

580

### 5. Conclusion

Since the beginning of the Industrial Revolution, growing human populations have resulted in increased waste production, agriculture, and the use of fossil fuels. Therefore, this study demonstrated the spatiotemporal dynamics of  $XCH_4$  in the atmosphere and associated natural (wetlands) and anthropogenic sources (coal fields and thermal power plants) in the Indian region. The present study utilized the remote sensing based  $XCH_4$  data from the GOSAT and S5P/TROPOMI from 2009 to 2022. The following are the salient findings of the study.

585

- The present study demonstrated the continuous  $XCH_4$  data from the S5P/TROPOMI and GOSAT to effectively monitor the  $XCH_4$  dynamics in space and time.
- Long-term trends of  $XCH_4$  show significant annual growth from 2009 to 2022 in  $CH_4$  over the Indian subcontinent, with a yearly growth rate of 8.76 ppb which is in line with the global trend.

590

- 595
- Long-term temporal and spatial distribution characteristics and variations of CH<sub>4</sub> emissions in India have accelerated in the last decade and globally, a substantial diffusion of CH<sub>4</sub> is observed from the northern to southern hemisphere.
  - XCH<sub>4</sub> levels peak in September-October over coal and thermal power plants but reach their minimum during March-May. The seasonal maxima of wetlands vary from site to site and are related to their size and active phase of methanogens.
  - Majority of the wetlands show an annual growth rate in XCH<sub>4</sub> is about 9.50 ppb year<sup>-1</sup>, indicates rich in moist habitats and active methanogens process.
  - High XCH<sub>4</sub> trend of 9.72±0.41 ppb year<sup>-1</sup> from the Mundra UMPP, Gujarat as well as the Paschim Bardhman coal mine (slope of 10.15±0.55 ppb year<sup>-1</sup>) indicated elevated and significant emissions from fossil fuel industries as compared to other natural sources.
  - The highest CH<sub>4</sub> emission estimate was observed during the monsoon season over the Sundarbans wetland, the largest protected wetland in India, with a maximum value of 23.62±3.66 mg m<sup>-2</sup> month<sup>-1</sup>. Among the wetland sites, Wular Lake has a rising methane rate of 0.04 mg m<sup>-2</sup> month<sup>-1</sup> with a p-value of 0.01.
  - The high levels of CH<sub>4</sub> emissions seen in the MGP, TGP, UGP, ECPH, LGP, and EGP agroclimatic zones may be related to the varied farming methods and traditional agricultural output in these regions. Most of these areas revolve around the Rice-Wheat farming system which is negatively impacting the climate.
  - The spatial patterns of XCH<sub>4</sub> concentrations agree well with the high-emission regions. The correlation coefficient 'r' is strongly agreed in the IGP region.

600

605

610

Therefore we conclude that the space based XCH<sub>4</sub> dataset provides significant support to track long-term changes in CH<sub>4</sub> and provides insightful information on the causes and feedback mechanisms for the elevated concentrations of methane across the south Asia region.

### Code and data availability

620 GOSAT (<https://data2.gosat.niesgo.jp/GosatDataArchive> Serv.ice/Usr) TROPOMI ([https://disc.gsfc.nasa.gov/datasets/S5P\\_L2\\_CH4\\_HiR\\_2](https://disc.gsfc.nasa.gov/datasets/S5P_L2_CH4_HiR_2)) satellite data, EDGAR bottom up inventory (<https://edgar.jrc.ec.europa.eu/gallery?release=v50&substance=CH4&sector=TOTALS>) and wetland methane emissions and uncertainty ([https://daac.ornl.gov/CMS/guides/MonthlyWetland\\_CH4\\_WetCHARTs.html](https://daac.ornl.gov/CMS/guides/MonthlyWetland_CH4_WetCHARTs.html)) data used in the present study are freely available and can be downloaded as summarised in figure 2 with the user's credentials. The code will be available from the author upon request.

625

### Declaration of Interest Statement

Authors declare no conflict of interest.

630

## Author Contribution

635 D.V. Mahalakshmi: Conceptualization, Formal analysis, Writing – original draft. Mahesh P:  
Conceptualization, Formal analysis, Writing – original draft. A.L.Kanchana: Conceptualization,  
Formal analysis, Writing – original draft. Sujatha. P: Formal data analysis, Writing – original  
draft. Ibrahim Shaik: Analysis. K.S. Rajan: Writing-review and Editing. Vijay Kumar Sagar:  
Formal Analysis and data curation. P. Raja: Writing-review and Editing. Y.K.Tiwari: Writing  
640 reviewing and Editing. Prakash Chauhan: Writing-review and Editing.

## Acknowledgement

We sincerely thank the Director, NRSC-ISRO, for his kind guidance and support. Authors  
greatly acknowledge the JAXA and National Institute of Environmental Studies (NIES) for  
645 providing free access to the GOSAT XCH<sub>4</sub> observations ([https://data2.gosat.niesgo.jp/GosatDataArchive\\_Serv.ice/usr/download](https://data2.gosat.niesgo.jp/GosatDataArchive_Serv.ice/usr/download) accessed on 15 June 2023) and the Earthdata for  
giving access to the S5P/TROPOMI ([https://disc.gsfc.nasa.gov/datasets/S5P\\_L2\\_CH4\\_HiR\\_2/summary](https://disc.gsfc.nasa.gov/datasets/S5P_L2_CH4_HiR_2/summary) accessed on 15 June 2023) data. We also thank the  
European Commission’s Joint Research Centre (JRC) for providing the CH<sub>4</sub> bottom-up  
650 inventory of EDGAR (<https://edgar.jrc.ec.europa.eu/gallery?release=v50&substance=CH4&sector=TOTALS>, accessed on 25 July 2023). The authors also thank the Oak Ridge  
National Laboratory (ORNL) Distributed Active Archive Center (DAAC) for providing the  
wetland methane emissions data. This work has been carried out as part of Technology  
Development Project (TDP) titled “Investigation of Atmospheric GHGs Emissions over the  
655 Indian Region (AGE)” and the Land- Ocean-Atmospheric GHGs Interaction Experiments  
(LOAGIN-X) of Climate and Atmospheric Processes of ISRO-Geosphere Biosphere programme  
(CAP-IGBP). We are very grateful to the anonymous reviewers and the handling editor for their  
constructive comments and suggestions, which have helped us to improve the manuscript.

## References

660

Ahmad, L., Kanth,R., Parvaze, S., and Mahdi, S.: Agro-climatic and Agro-ecological Zones of  
India. In: *Experimental Agrometeorology: A Practical Manual*. Springer, Cham., 99-118,  
[https://doi.org/10.1007/978-3-319-69185-5\\_15](https://doi.org/10.1007/978-3-319-69185-5_15), 2017.

665

Balcombe, P., Speirs, J.F., Brandon, N. P., and Hawkes, A. D.: Methane emissions: Choosing  
the right climate metric and time horizon, *Environ Sci Process Impacts*, 20(10), 1323–1339,  
<https://doi.org/10.1039/C8EM00414E>, 2018.

- 670 Bassi, N., Dinesh, K.M., Anuradha, S., and PardhaSaradhi, P.: Status of wetlands in India: A review of extent, ecosystem benefits, threats and management strategies, *J. Hydrol. Reg. Stud* 2, 1, 2014.
- 675 Behera, M.D., Mudi, S., Shome, P., Das, P.K., Kumar, S., Joshi, A., Rathore, A., Deep, A., Kumar, A., Sanwariya, C. and Kumar, N.: COVID-19 slowdown induced improvement in air quality in India: Rapid assessment using Sentinel-5P TROPOMI data, *Geocarto International*, 37(25), 8127-8147. <https://doi.org/10.1080/10106049.2021.1993351>, 2022.
- 680 Bloom, A. A., K. W. Bowman, M. Lee, A. J. Turner, R. Schroeder, J. R. Worden, R. Weidner, K. C. McDonald, and D. J. Jacob.: A global wetland methane emissions and uncertainty dataset for atmospheric chemical transport models (WetCHARTs version 1.0), *Geosci. Model Dev.*, 10, 2141–2156, <https://doi.org/10.5194/gmd-10-2141-2017>, 2017a.
- Bloom, A. A., K. Bowman, M. Lee, A. J. Turner, R. Schroeder, J. R. Worden, R. J. Weidner, K. C. McDonald, and D. J. Jacob.: CMS: Global 0.5-deg Wetland Methane Emissions and Uncertainty (WetCHARTs v1.0), ORNL DAAC, Oak Ridge, Tennessee, USA,
- 685 <https://doi.org/10.3334/ORNLDAAC/1502>, 2017b.
- Bloom, A.A., K.W. Bowman, M. Lee, A.J. Turner, R. Schroeder, J.R. Worden, R.J. Weidner, K.C. McDonald, and D.J. Jacob.: CMS: Global 0.5-deg Wetland Methane Emissions and Uncertainty (WetCHARTs v1.3.1), ORNL DAAC, Oak Ridge, Tennessee, USA, <https://doi.org/10.3334/ORNLDAAC/1915>, 2021.
- 690 Bussmann, I., Achterberg, E.P., Brix, H., Brüggemann, N., Flöser, G., Schütze, C. and Fischer, P.: Influence of wind strength and direction on diffusive methane fluxes and atmospheric methane concentrations above the North Sea. *Biogeosciences*, 21(16), 3819-3838 <https://doi.org/10.5194/egusphere-2023-3018>, 2024.
- 695 Chandra, N., Hayashida, S., Saeki, T., and Patra, P. K.: What controls the seasonal cycle of columnar methane observed by GOSAT over different regions in India?, *Atmospheric Chemistry and Physics*, 17(20), 12633-12643. <https://doi.org/10.5194/acp-17-12633-2017>, 2017.
- 700 Choudhary, B.B., and Sirohi, S.: Understanding vulnerability of agricultural production system to climatic stressors in North Indian Plains: a meso-analysis, *Environ Dev Sustain*, 24, 13522–13541, <https://doi.org/10.1007/s10668-021-01997-7>, 2022.
- 705 Crippa, M., Solazzo, E., Huang, G., Guizzardi, D., Koffi, E., Muntean, M., Schieberle, C., Friedrich, R. and Janssens-Maenhout, G.: High resolution temporal profiles in the Emissions Database for Global Atmospheric Research, *Scientific data*, 7(1), p.121, 2020.

- 710 Crutzen, P.J. and Zimmermann, P.H.: The changing photochemistry of the troposphere. *Tellus B: Chem. Phys. Meteorol.* 43(4), 136-151 <https://doi.org/10.3402/tellusb.v43i4.15403>, 1991.
- Feng, L., Palmer, P.I., Zhu, S., Parker, R.J. and Liu, Y.: Tropical methane emissions explain large fraction of recent changes in global atmospheric methane growth rate, *Nat. Commun.*, 13(1),1378, <https://doi.org/10.1038/s41467-022-28989-z>, 2022.
- 715 Feng, L., Palmer, P. I., Parker, R. J., Lunt, M. F., and Bösch, H.: Methane emissions are predominantly responsible for record-breaking atmospheric methane growth rates in 2020 and 2021. *Atmos. Chem. Phys.*, 23, 4863–4880, <https://doi.org/10.5194/acp-23-4863-2023>, 2023.
- 720 [Francis, D., Weston, M., Fonseca, R., Temimi, M. and Alsuwaidi, A.: Trends and variability in methane concentrations over the Southeastern Arabian Peninsula. \*Front. Environ. Sci.\*, 11:1177877, <https://doi.org/10.3389/fenvs.2023.1177877>, 2023.](https://doi.org/10.3389/fenvs.2023.1177877)
- 725 Frankenberg, C., Aben, I. P. B. J. D. E., Bergamaschi, P., Dlugokencky, E. J., Van Hees, R., Houweling, S., P. Van Der Meer, R. Snel, and Tol, P.: Global column-averaged methane mixing ratios from 2003 to 2009 as derived from SCIAMACHY: Trends and variability, *J. Geophys. Res. Atmos.*, 116(D4), <https://doi.org/10.1029/2010JD014849>, 2011.
- 730 Fu, B., Jiang, Y., Chen, G., Lu, M., Lai, Y., Suo, X., and Li, B.: Unraveling the dynamics of atmospheric methane: the impact of anthropogenic and natural emissions, *Environ. Res. Lett.*, 19 064001 , [10.1088/1748-9326/ad4617](https://doi.org/10.1088/1748-9326/ad4617), 2024.
- 735 Ganesan, A. L., Schwietzke, S., Poulter, B., Arnold, T., Lan, X., Rigby, M., Vogel, F. R., van der Werf, G. R., Janssens-Maenhout, G., Boesch, H., Pandey, S., Manning, A. J., Jackson, R. B., Nisbet, E. G., and Manning, M. R.: Advancing scientific understanding of the global methane budget in support of the Paris Agreement, *Global Biogeochem. Cy.*, 33, 1475–1512, <https://doi.org/10.1029/2018GB006065>, 2019.
- 740 Hayashida, S., Ono, A., Yoshizaki, S., Frankenberg, C., Takeuchi, W., and Yan, X.: Methane concentrations over Monsoon Asia as observed by SCIAMACHY: signals of methane emission from rice cultivation, *Remote Sens. Environ.*, 139, 246–256, <https://doi.org/10.1016/j.rse.2013.08.008>, 2013.
- 745 Huang, L., Tang, M., Fan, M., and Cheng, H.: Density functional theory study on the reaction between hematite and methane during chemical looping process, *Applied Energy*, 159, 132-144, <https://doi.org/10.1016/j.apenergy.2015.08.11> , 2015.

- 750 IPCC: Climate change.: The physical science basis, Contribution of Working Group I to the sixth assessment report of the intergovernmental panel on climate change, 2021.
- Kang, M., Mauzerall, D. L., Ma, D. Z., and Celia, M. A.: Reducing methane emissions from abandoned oil and gas wells: Strategies and costs. *Energy Policy*, 132, 594-601, <https://doi.org/10.1016/j.enpol.2019.05.045>, 2019.
- 755 Kavitha, M., and Nair, P. R.: Region-dependent seasonal pattern of methane over Indian region as observed by SCIAMACHY, *Atmos. Environ*, 131, 316-325 <https://doi.org/10.1016/j.atmosenv.2016.02.008>, 2016.
- 760 Kavitha, M., Nair, P. R., Girach, I. A., Aneesh, S., Sijikumar, S., and Renju, R.: Diurnal and seasonal variations in surface methane at a tropical coastal station, Role of mesoscale meteorology, *Sci. Total Environ*. 631, 1472-1485, <https://doi.org/10.1016/j.scitotenv.2018.03.123> 2018.
- 765 Kirschke, S., Bousquet, P., Ciais, P., Saunois, M., Canadell, J. G., Dlugokencky, E. J., Bergamaschi, P., Bergmann, D., Blake, D. R., Bruhwiler, L., Cameron-Smith, P., Castaldi, S., Chevallier, F., Feng, L., Fraser, A., Heimann, M., Hodson, E. L., Houweling, S., Josse, B., Fraser, P. J., Krummel, P. B., Lamarque, J.- F., Langenfelds, R. L., Quéré, C. L., Naik, V., O'Doherty, S., Palmer, P. I., Pison, I., Plummer, D., Poulter, B., Prinn, R. G., Rigby, M., Ringeval, B., Santini, M., Schmidt, M., Shindell, D. T., Simpson, I. J., Spahni, R., Steele, L. P., 770 Strode, S. A., Sudo, K., Szopa, S., Werf, G. R. van der, Voulgarakis, A., Weele, M. van, Weiss, R. F., Williams, J. E., and Zeng, G.: Three decades of global methane sources and sinks, *Nat. Geosci.*, 6, 1–11, <https://doi.org/10.1038/ngeo1955>, 2013.
- 775 Kozicka, K., Orazalina, Z., Gozdowski, D., and Wójcik-Gront, E.: Evaluation of temporal changes in methane content in the atmosphere for areas with a very high rice concentration based on Sentinel-5P data, *Remote Sens. Appl.: Soc. Environ*, 30, 100972, <https://doi.org/10.1016/j.rsase.2023.100972>, 2023.
- 780 Kuze, A., Suto, H., Nakajima, M. and Hamazaki, T.: Thermal and near infrared sensor for carbon observation Fourier-transform spectrometer on the Greenhouse Gases Observing Satellite for greenhouse gases monitoring. *Appl. Opt.* 48(35),6716-6733, <https://doi.org/10.1364/AO.48.006716>, 2009.
- 785 Lan, X., K.W. Thoning, and E.J. Dlugokencky.: Trends in globally-averaged CH<sub>4</sub>, N<sub>2</sub>O, and SF<sub>6</sub> determined from NOAA Global Monitoring Laboratory measurements, Version 2024-01, <https://doi.org/10.15138/P8XG-AA10>.



Lorente, A., Borsdorff, T., Butz, A., Hasekamp, O., Aan De Brugh, J., Schneider, A., Wu, Lianghai., Hase, F., Kivi, R., Wunch, D., Pollard, D.F., Shiomi, K., Deutscher, N.M., Velazco,

790 Lu, X., Jacob, D.J., Zhang, Y., Shen, L., Sulprizio, M.P., Maasackers, J.D., Varon, D.J., Qu, Z., Chen, Z., Hmiel, B. and Parker, R.J.: Observation-derived 2010-2019 trends in methane emissions and intensities from US oil and gas fields tied to activity metrics. *Proceedings of the National Academy of Sciences*, 120(17), e2217900120, 2023.

795 Maasackers, J. D., McDuffie, E. E., Sulprizio, M. P., Chen, C., Schultz, M., Brunelle, L., Thrush, R., Steller, J., Sherry, C., Jacob, D.J., Jeong, S., Irving, B., and Weitz, M.. A gridded inventory of annual 2012–2018 US anthropogenic methane emissions. *Environ. Sci. Technol.*, 57(43), 16276-16288, 2023.

800 Nair, P. R., and Kavitha, M.: Stratospheric distribution of methane over a tropical region as observed by MIPAS on board ENVISAT, *Int. J. Remote Sens.*, 41(21), 8380-8405, 2020.

Pai, S., and Zeriffi, H.: A novel dataset for analysing sub-national socioeconomic developments in the Indian coal industry, *IOP SciNotes*, vol. 2, no. 1, p. 014001, Mar. 2021, doi: 10.1088/2633-1357/abdbbb.

810 Parker, R. J., Boesch, H., McNorton, J., Comyn-Platt, E., Gloor, M., Wilson, C., Chipperfield, M.P., Hayman, G.D., and Bloom, A. A.: Evaluating year-to-year anomalies in tropical wetland methane emissions using satellite CH<sub>4</sub> observations. *Remote Sens. Environ.*, 211, 261-275. <https://doi.org/10.1016/j.rse.2018.02.011>, 2018.

815 Pathakoti, M., Santhoshi, T., Aarathi, M., Mahalakshmi, D.V., Kanchana, A.L., Srinivasulu, J., SS, R.S., Soni, V.K., MVR, S.S. and Raja, P.: Assessment of spatio-temporal climatological trends of ozone over the Indian region using machine learning, *Spat. Stat.*, 43,100513. [10.1016/j.spasta.2021.100513](https://doi.org/10.1016/j.spasta.2021.100513), 2021.

Peng, S., Lin, X., Thompson, R.L., Xi, Y., Liu, G., Hauglustaine, D., Lan, X., Poulter, B., Ramonet, M., Saunoy, M. and Yin, Y.: Wetland emission and atmospheric sink changes explain methane growth in 2020. *Nature*, 612(7940), 477-482, 2022.

820 [Ricaud, P., Sič, B., El Amraoui, L., Attié, J.L., Zbinden, R., Huszar, P., Szopa, S., Parmentier, J., Jaidan, N., Michou, M. and Abida, R.: Impact of the Asian monsoon anticyclone on the variability of mid-to-upper tropospheric methane above the Mediterranean Basin. \*Atmos. Chem. Phys.\*, 14\(20\), 11427-11446, <https://doi.org/10.5194/acp-14-11427-2014>, 2014.](https://doi.org/10.5194/acp-14-11427-2014)

- Rocher-Ros, G., Stanley, E.H., Loken, L.C., Casson, N.J., Raymond, P.A., Liu, S., Amatulli, G. and Sponseller, R.A.: Global methane emissions from rivers and streams, *Nature*, 621(7979), pp.530-535, <https://doi.org/10.1038/s41586-023-06344-6>, 2023.
- 830 Salimi, S., Almuktar, S.A., and Scholz, M.: Impact of climate change on wetland ecosystems: A critical review of experimental wetlands, *J. Environ. Manage.*, <https://doi.org/10.1016/j.jenvman.2021.112160>, 2021.
- 835 Sagar, V. K., Pathakoti, M., Mahalakshmi, D. V., Rajan, K. S., MVR, S. S., Hase, F., ... & Sha, M. K.: Ground-Based Remote Sensing of Total Columnar CO<sub>2</sub>, CH<sub>4</sub>, and CO Using EM27/SUN FTIR Spectrometer at a Suburban Location (Shadnagar) in India and Validation of Sentinel-5P/TROPOMI, *IEEE Geoscience and Remote Sensing Letters*, 19, 1-5. [10.1109/LGRS.2022.3171216](https://doi.org/10.1109/LGRS.2022.3171216), 2022.
- 840 Sakalli, A., Cescatti, A., Dosio, A., and Gücel, M. U.: Impacts of 2°C global warming on primary production and soil carbon storage capacity at pan-European level, *Climate Services*, 7, 64-77, 2017.
- 845 Saunio, M., Bousquet, P., Poulter, B., Peregon, A., Ciais, P., Canadell, J. G., Dlugokencky, E. J., Etiope, G., Bastviken, D., Houweling, S., Janssens-Maenhout, G., Tubiello, F. N., Castaldi, S., Jackson, R. B., Alexe, M., Arora, V. K., Beerling, D. J., Bergamaschi, P., Blake, D. R., Brailsford, G., Brovkin, V., Bruhwiler, L., Crevoisier, C., Crill, P., Covey, K., Curry, C., Frankenberg, C., Gedney, N., Höglund-Isaksson, L., Ishizawa, M., Ito, A., Joos, F., Kim, H.-S., Kleinen, T., Krummel, P., Lamarque, J.-F., Langenfelds, R., Locatelli, R., Machida, T., Maksyutov, S., McDonald, K. C., Marshall, J., Melton, J. R., Morino, I., Naik, V., O'Doherty, S., Parmentier, F.-J. W., Patra, P. K., Peng, C., Peng, S., Peters, G. P., Pison, I., Prigent, C., Prinn, R., Ramonet, M., Riley, W. J., Saito, M., Santini, M., Schroeder, R., Simpson, I. J., Spahni, R., Steele, P., Takizawa, A., Thornton, B. F., Tian, H., Tohjima, Y., Viovy, N., Voulgarakis, A., van Weele, M., van der Werf, G. R., Weiss, R., Wiedinmyer, C., Wilton, D. J., Wiltshire, A., Worthy, D., Wunch, D., Xu, X., Yoshida, Y., Zhang, B., Zhang, Z., and Zhu, Q.: The global methane budget 2000–2012, *Earth Syst. Sci. Data*, 8, 697–751, <https://doi.org/10.5194/essd-8-697-2016>, 2016.
- 850
- 855 Saunio, M., Martinez, A., Poulter, B., Zhang, Z., Raymond, P., Regnier, P., Canadell, J. G., Jackson, R. B., Patra, P. K., Bousquet, P., Ciais, P., Dlugokencky, E. J., Lan, X., Allen, G. H., Bastviken, D., Beerling, D. J., Belikov, D. A., Blake, D. R., Castaldi, S., Crippa, M., Deemer, B. R., Dennison, F., Etiope, G., Gedney, N., Höglund-Isaksson, L., Holgerson, M. A., Hopcroft, P. O., Hugelius, G., Ito, A., Jain, A. K., Janardanan, R., Johnson, M. S., Kleinen, T., Krummel, P., Lauerwald, R., Li, T., Liu, X., McDonald, K. C., Melton, J. R., Mühle, J., Müller, J., Murguia-
- 865

Flores, F., Niwa, Y., Noce, S., Pan, S., Parker, R. J., Peng, C., Ramonet, M., Riley, W. J., Rocher-Ros, G., Rosentreter, J. A., Sasakawa, M., Segers, A., Smith, S. J., Stanley, E. H., Thanwerdas, J., Tian, H., Tsuruta, A., Tubiello, F. N., Weber, T. S., van der Werf, G., Worthy, D. E., Xi, Y., Yoshida, Y., Zhang, W., Zheng, B., Zhu, Q., Zhu, Q., and Zhuang, Q.: Global Methane Budget 2000–2020, *Earth Syst. Sci. Data Discuss.* [preprint],  
870 <https://doi.org/10.5194/essd-2024-115>, in review, 2024.

Schaefer, H., Fletcher, S. E. M., Veidt, C., Lassey, K. R., Brailsford, G. W., Bromley, T. M., Dlugokencky, E. J., Michel, S. E., Miller, J. B., Levin, I., Lowe, D. C., Martin, R. J., Vaughn, B.  
875 H., and White, J. W. C.: A 21st century shift from fossil-fuel to biogenic methane emissions indicated by  $^{13}\text{CH}_4$ , *Science*, 352, <https://doi.org/10.1126/science.aad2705>, 2016.

Schneising, O., Buchwitz, M., Burrows, J. P., Bovensmann, H., Bergamaschi, P., and Peters, W.: Three years of greenhouse gas column-averaged dry air mole fractions retrieved from satellite –  
880 Part 2: Methane, *Atmos. Chem. Phys* 9, 443–465, doi:10.5194/acp-9-443-2009, 2009.

Shaw, J.T., Allen, G., Barker, P., Pitt, J.R., Pasternak, D., Bauguitte, S.J.B., Lee, J., Bower, K.N., Daly, M.C., Lunt, M.F., Ganesan, A.L., Vaughan, A.R., Chibesankunda, F., Lambakasa, M., Fisher, R.E., France, J.L., Lowry, D., Palmer, P.I., Metzger S., Parker, R.J., Gedney, N.,  
885 Bareson, P., Cain, M., Lorente, A., Borsdorff, T., Nisbet, E.G.: Large Methane Emission Fluxes Observed from Tropical Wetlands in Zambia.: <https://doi.org/10.1029/2021GB007261>, 2022.

Song, H., Sheng, M., Lei, L., Guo, K., Zhang, S. and Ji, Z.: Spatial and Temporal Variations of Atmospheric  $\text{CH}_4$  in Monsoon Asia Detected by Satellite Observations of GOSAT and  
890 TROPOMI. *Remote Sensing*, 15(13), 3389, <https://doi.org/10.3390/rs15133389>, 2023.

Sreenivas, G., Mahesh, P., Subin, J., Kanchana, A. L., Rao, P. V. N., and Dadhwal, V. K.: Influence of meteorology and interrelationship with greenhouse gases ( $\text{CO}_2$  and  $\text{CH}_4$ ) at a suburban site of India, *Atmos. chem. phys.*, 16, 3953-3967, doi.org/10.5194/acp-16-3953-2016,  
895 2016.

Sreenivas, G., Mahesh, P., Mahalakshmi, D.V., Kanchana, A.L., Naveen Chandra, Prabir K. Patra, Raja, P., Shesha Sai M.V.R., Sripada, S., Rao, P.V., and Dadhwal, V.K.: Seasonal and annual variations of  $\text{CO}_2$  and  $\text{CH}_4$  at Shadnagar, a semi-urban site, *Sci. Total Environ.*, 819:153114, <https://doi.org/10.1016/j.scitotenv.2022.153114>, 2022.  
900

Taneja, G., Pal, B.D., Joshi, P.K., Aggarwal, P.K. and Tyagi, N.K.: Farmers' preferences for climate-smart agriculture—an assessment in the Indo-Gangetic Plain (pp. 91-111). Springer Singapore, 2019.  
905

- Turner, A. J., Frankenberg, C., and Kort, E. A.: Interpreting contemporary trends in atmospheric methane, *P. Natl. Acad. Sci. USA*, 116, 2805–2813, <https://doi.org/10.1073/pnas.1814297116>, 2019
- 910 Vinna, L., Medhaug, I., and Schmid, M.: The vulnerability of lakes to climate change along an altitudinal gradient. *Commun. Earth Environ.* 2, 35. <https://doi.org/10.1038/s43247-021-00106-w>,2021.
- 915 Wang, Y., Yang, H., Ye, C., Chen, X., Xie, B., Huang, C., Zhang, J. and Xu, Mx.: Effects of plant species on soil microbial processes and CH<sub>4</sub> emission from constructed wetlands. *Environ. Pollut.*, 174, 273-278, 2013.
- Wei,Y., Yang, X., Qiu, X., Wei, H., and Tang, C.: Spatio-temporal variations of atmospheric methane and its response to climate on the Tibetan Plateau from 2010 to 2022, *Atmos. Environ.*, <https://doi.org/10.1016/j.atmosenv.2023.120088>, 2023.
- 920 Worden, J. R., Bloom, A. A., Pandey, S., Jiang, Z., Worden, H. M., Walker, T. W., Houweling, S., and Röckmann, T.: Reduced biomass burning emissions reconcile conflicting estimates of the post-2006 atmospheric methane budget, *Nat. Commun.*, 8, 1–11, <https://doi.org/10.1038/s41467-017-02246-0>, 2017.
- 925 Zhang, L., Tian, H., Shi, H., Pan, S., Chang, J., Dangal, S. R., ... & Jackson, R. B.: A 130-year global inventory of methane emissions from livestock: Trends, patterns, and drivers. *Global Change Biology*, 28(17), 5142-5158, <https://doi.org/10.1111/gcb.16280>, 2022.
- 930 Zhang, Z., Poulter, B., Feldman, A.F., Ying, Q., Ciais, P., Peng, S. and Li, X.: Recent intensification of wetland methane feedback. *Nature Climate Change*, 13(5), pp.430-433. <https://doi.org/10.1038/s41558-023-01629-0>, 2023.